Application Note

Custom Steering Vectors for the IWRL6432AOP

Nathan Block

ABSTRACT

The IWRL6432AOP is a low-power, highly integrated radar chip that uses 60GHz radiation to effectively detect, localize, track and classify human and non-human targets over a large field of view. The IWRL6432AOP can be used to turn on a video camera, power on an air conditioner, or prevent a robot from colliding with a person when the robot determines someone is present. To detect presence accurately though, the IWRL6432AOP need to be able to localize people effectively in 3D space. TI offers two angle-of-arrival (AOA) estimation algorithms to accomplish this. For power-constrained applications, the FFT beamforming algorithm delivers AOA estimation results with an average absolute error of 8.5° within a ±60° FOV. Alternatively, for devices with a higher power budget, the steering vectors beamforming algorithm achieves an average absolute error of 2.9° within a ±70° FOV, and takes 0.15 additional msec per detected point. This application note discusses the theory behind both methods, the tradeoffs between the methods, and the results when the methods were tested in the lab and outdoors.

Table of Contents

Trademarks

1 Introduction

1.1 Angle of Arrival Estimation Theory: FFT Beamformer

Based off the theory in The Fundamentals of Millimeter Wave Radar Sensors, the angle of arrival of an object in the FOV in the radar can be estimated using Equation 1 and Equation 2.

$$\Delta\Phi = \frac{2\pi\Delta d}{\lambda} \tag{1}$$

If all the antennas are aligned in a planar wave-front, then basic geometry shows that Δd = lsin(θ)

$$\theta = \sin^{-1}\left(\frac{\lambda\Delta\Phi}{2\pi l}\right) \tag{2}$$

In practice, MIMO systems use more than two antennas though, so the change in phase (ΔΦ) is not just a change in phase across two antennas, but change in phase across N-antennas. Change in phase over space is known as spatial frequency (ω), and this can be estimated using an FFT.

$$\theta = \sin^{-1}\left(\frac{\lambda\Delta\Phi}{2\pi l}\right) = \sin^{-1}\left(\frac{\lambda\omega}{2\pi l}\right) \tag{3}$$

The FFT is often padded with a large number of zeros to increase the number of candidate angles (seen on the X-axis). As a result, the angle FFT often produce broad peaks. Therefore, to estimate the angle-of-arrival of an object, the radar compares the magnitude of the FFT at all these different candidate locations, and select the peak (or peaks) that correspond to the maximum values in the angle-spectrum. The picture below illustrates this, and the selected peak is at index 11, since the magnitude is highest.

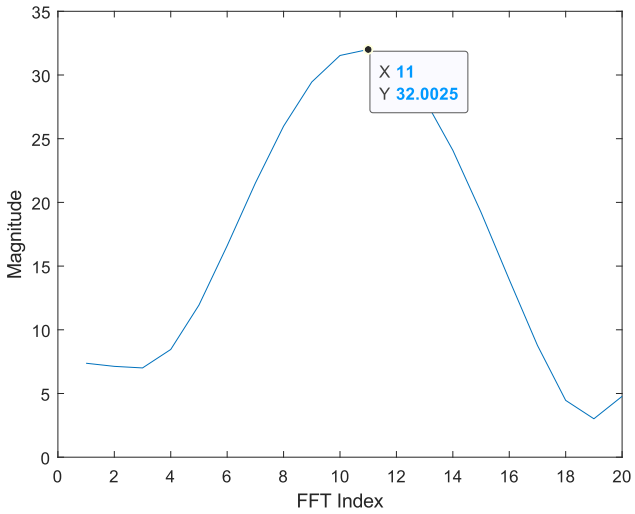

Figure 1-1. Broad FFT Spectrum with Max Peak at Index 11

On the IWRL6432, this FFT calculation is done using the radar hardware accelerator. However, this is fundamentally equivalent to a matrix-vector product of the FFT matrix with the received phase of all the antennas. The AOA that is selected is the angle which corresponds to the maximum value of a_i in Equation 4.

$$\begin{pmatrix} \boldsymbol{w}^0 & \boldsymbol{w}^0 & \cdots & \boldsymbol{w}^0 \\ \boldsymbol{w}^0 & \boldsymbol{\omega}^1 & \cdots & \boldsymbol{\omega}^{N-1} \\ \vdots & \cdots & \ddots & \vdots \\ \boldsymbol{w}^0 & \boldsymbol{\omega}^{N-1} & \cdots & \boldsymbol{\omega}^{(N-1)(N-1)} \end{pmatrix} \begin{pmatrix} \boldsymbol{\phi}_0 \\ \boldsymbol{\phi}_1 \\ \cdots \\ \boldsymbol{\phi}_{N-1} \end{pmatrix} = \begin{pmatrix} \boldsymbol{a}_0 \\ \boldsymbol{a}_1 \\ \cdots \\ \boldsymbol{a}_{N-1} \end{pmatrix} \tag{4}$$

$$\omega = e^{\frac{-j2\pi}{N}} \tag{5}$$

From the vector of output correlation vector x, select the FFT index that corresponds to the maximum value of x_i.

$$idx_{est} = argmax_i(a_i) \tag{6}$$

Then, use the AOA formula to compute the estimated AOA θ_{est}.

$$if\left(idx_{est} \leq \frac{N}{2}\right) \rightarrow \theta_{est} = \text{asin}\left(\frac{2 \times idx_{est}}{N}\right) \tag{7}$$

$$if\left(idx_{est} > \frac{N}{2}\right) \rightarrow \theta_{est} = \text{asin}\left(\frac{N - 2 \times idx_{est}}{N}\right) \tag{8}$$

1.2 Angle of Arrival Estimation Theory: Steering Vectors

The equations above and the FFT are estimates of the angle of arrival of different objects. Unfortunately, if there are non-linearities in the radar or antennas, or gain/phase mismatch in each individual antenna, then the FFT-matrix and equations above do not accurately estimate the angle of arrival of the object. An alternative design here is to recompute the FFT matrix experimentally by measuring the returned phase of the radar signal for targets swept over all potential angles of arrival, and using these coefficients as the ground-truth vectors. This is what is known as the *steering vector* algorithm for the IWRL6432AOP.

$$\begin{pmatrix} \boldsymbol{x}_{11} & \boldsymbol{x}_{12} & \cdots & \boldsymbol{x}_{1N} \\ \boldsymbol{x}_{21} & \boldsymbol{x}_{22} & \cdots & \boldsymbol{x}_{2N} \\ \vdots & \cdots & \ddots & \vdots \\ \boldsymbol{x}_{N-1,1} & \boldsymbol{x}_{N-1,2} & \cdots & \boldsymbol{x}_{N-1,N-1} \end{pmatrix} \begin{pmatrix} \boldsymbol{\phi}_0 \\ \boldsymbol{\phi}_1 \\ \ldots \\ \boldsymbol{\phi}_{N-1} \end{pmatrix} = \begin{pmatrix} \boldsymbol{a}_0 \\ \boldsymbol{a}_1 \\ \ldots \\ \boldsymbol{a}_{N-1} \end{pmatrix}$$

$$idx_{est} = argmax_i(a_i) \tag{9}$$

Based off the collected dataset (which sweeps the FOV in regular increments), θ_{est} is referenced in a look up table that maps the a indices to θ indices.

Table 1-1. Steering Vector Lookup Table Example

a	θ
0	-80°
1	-75°
2	-70°
…	…
N-1	80°

2 Additional Information

2.1 Measurement Procedure

To compute the Steering Vector Coefficient Matrix, TI measured the returned phase of the IWRL6432 over multiple PCB designs, units and temperatures. Using a Millibox miniature anechoic chamber and a corner reflector placed at a known distance from the radar, TI rotated the radar devices over a sweep of azimuth and elevation angles, and recorded the returned ADC data at each angle.

Figure 2-1 and Figure 2-2 show the setup that TI used with the radar on one end of the chamber and a corner reflector at the other end.

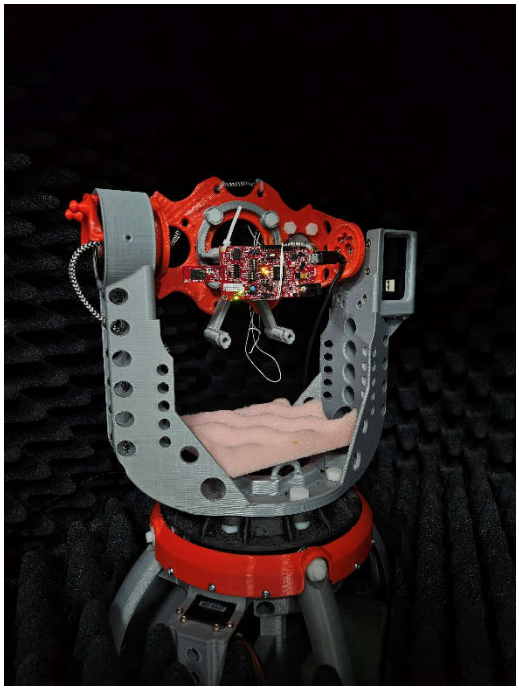

Figure 2-1. IWRL6432AOPEVM in Millibox Chamber

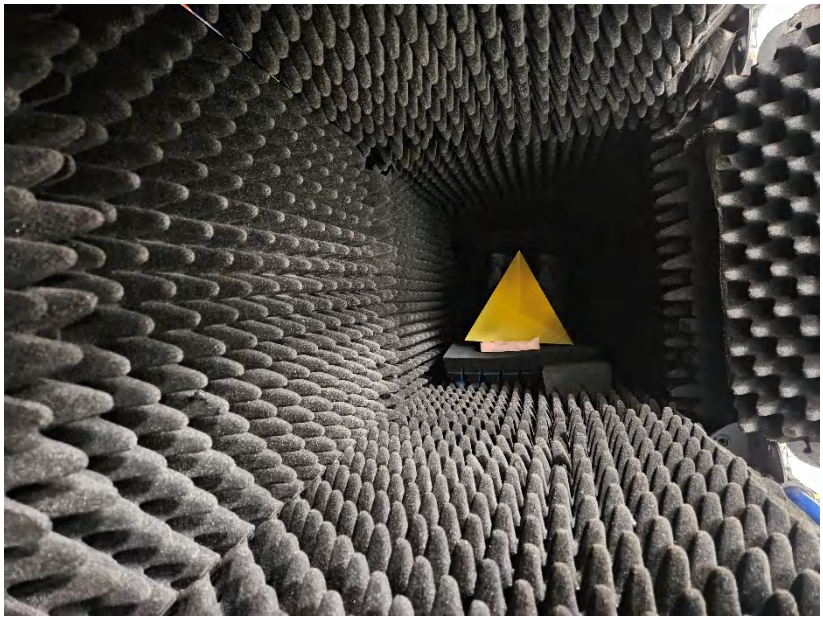

Figure 2-2. Corner Reflector at the Opposite End of Millibox Chamber

2.2 Testing Results

2.2.1 Anechoic Chamber Testing on Corner Reflector Targets

Using the results from the Millibox measurements, TI developed the steering vector algorithm to decode the angle of arrival with a greater degree of accuracy, and validated the performance on the algorithm on a different set of IWRL6432AOPEVMs devices. TI tested the devices over four different chirping profiles of varying bandwidths and start frequencies, and in two environments: first in the anechoic chamber on a corner reflector, then afterwards outdoors on a real person walking towards and away from the radar. The below table shows the chirping parameters.

Note that the steering vector algorithm works over the entire 57-63.5GHz bandwidth of the IWRL6432AOP device. The below chirps were selected as a sample of the potential chirps within this band.

Table 2-1. Chirp Bandwidth Used for Testing

Configuration #	Start Frequency (GHz)	End Frequency (GHz)
1	60.5	61.35
2	57	57.85
3	58.5	61.05
4	60	63.4

In the anechoic chamber, the steering vectors algorithm reduced the AOA estimation error throughout the entire field of view.

Table 2-2. AOA Error vs Azimuth Angle for FFT and SV Algorithms, Corner Reflector in Anechoic Chamber, Elevation = 0°

	-70°	-60°	-45°	-30°	0°	+30°	+45°	+60°	+70°
CFG # 1 (FFT)	44.5°	-5.2°	-3.4°	-6.8°	-0.5°	-0.9°	-5.8°	12.1°	-13.2°
Cfg #1 (Steering Vectors)	1.2°	1.7°	3.9°	-1.0°	0.2°	1.6°	3.1°	10.4°	-4.9°
Cfg #2 (FFT)	-20°	-10.4°	-4.4°	-6.9°	-2.9°	-2.5°	-5.3°	-10.1°	-10°
Cfg #2 (Steering Vectors)	0.4°	-3.2°	-1.4°	-3.1°	-1.8°	0.2°	4.1°	-5.3°	-6.7°
Cfg #3 (FFT)	-9.5°	-1.2°	-6.2°	-6.0°	-1.9°	-1.3°	-2.7°	-13.1°	-15.2°
Cfg #3 (Steering Vectors)	7.4°	5.7°	1.5°	-0.1°	0.1°	5.4°	5.6°	0.7°	-3.9°
Cfg #4 (FFT)	-4°	-4.8°	-4.1°	-6.2°	-1.4°	-1.2°	-5.0°	-45.4°	-13.8°
Cfg #4 (Steering Vectors)	3°	1.7°	1.3°	-1°	-0.1°	1.9°	4.5°	1.7°	-3.8°

2.2.2 Outdoor Testing on Human Subjects

Similar experiments were conducted in an outdoor environment on human subjects to make sure that the steering vectors package estimated AOA accurately in realistic scenarios too. The experimenter walked towards and away from the radar at a series of known angles, and the point cloud was collected for each trial. The average AOA error for all the points is shown in Figure 2-3 and Figure 2-3, and plots of all the trials can be found in the Appendix.

Table 2-3. AOA Error vs Azimuth Angle for FFT and SV Algorithms, Human Subject Walking Outdoors

	-70°	-60°	-45°	-30°	0°	30°	45°	60°	70°
Cfg #1 (FFT)	-12.5°	5.5°	6.6°	3.7°	1.5°	2.2°	7.1°	6.3°	-12.5°
Cfg #1 (Steering Vectors)	-6.5°	-2.6°	-2.3°	-2.1°	1.4°	0.8°	-0.7°	3.1°	-6.5°
Cfg #2 (FFT)	7.4°	9.9°	5.3°	6.0°	5.0°	2.0°	8.5°	5.7°	10.8°
Cfg #2 (Steering Vectors)	0.9°	4.2°	2.1°	3.3°	3.5°	-2.1°	-0.6°	-0.6°	3.2°
Cfg #3 (FFT)	2.4°	11.1°	10.5°	6.8°	3.5°	1.2°	9.3°	10.1°	2.4°
Cfg #3 (Steering Vectors)	-4.2°	0.3°	2.3°	0.2°	2.4°	-0.5°	1.4°	1.2°	-4.2°
Cfg #4 (FFT)	-16.7°	6.7°	6.1°	5.3°	3.6°	3.8°	9.7°	8.7°	9.4°
Cfg #4 (Steering Vectors)	-4.1°	-1.2°	-3.8°	-0.1°	2.8°	1.7°	0.3°	0.1°	2.7°

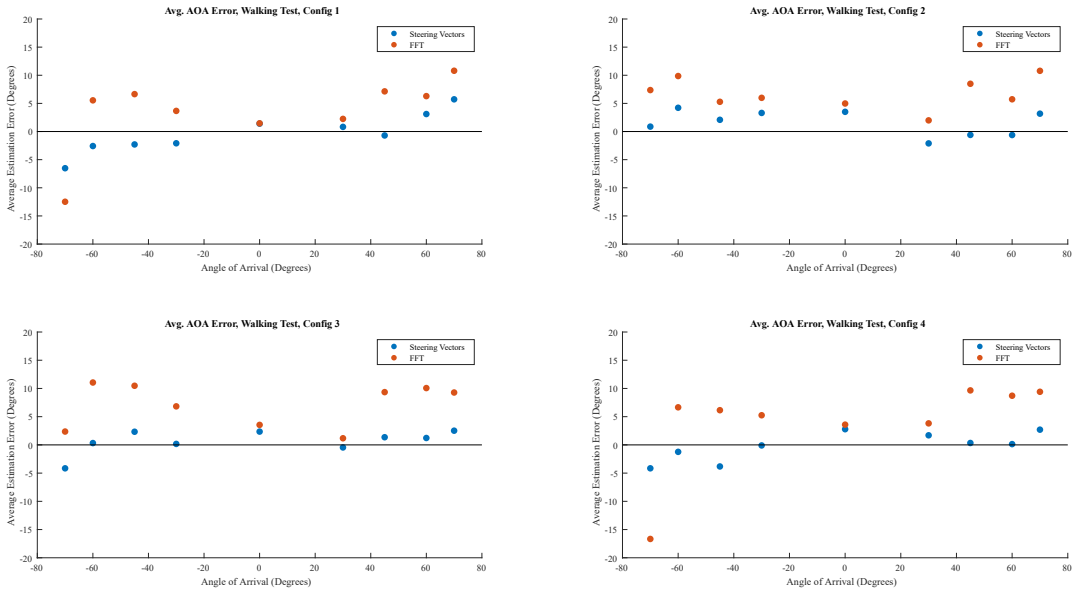

Figure 2-3. Walking Test AOA Error

Figure 2-4 shows the setup that is used to capture the data.

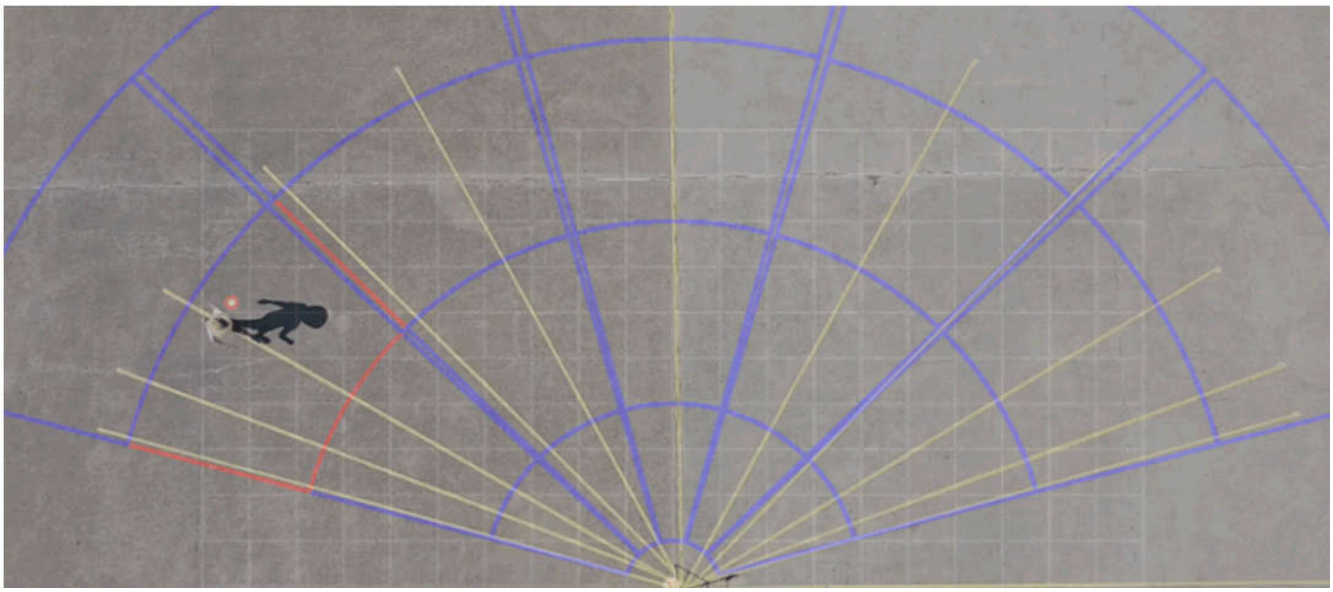

Figure 2-4. Walk Testing Environment (Bird's Eye View)

2.3 Processing Time

The AOA improvement from using the steering vectors package requires some additional processing to provide best performance. The increase in processing time can be quantified per-detected point, as the steering vector package runs only on the range bins with detected points. A breakdown of this timing can be seen below, and this results in approximately 150µsec per detected point with an added 676µsec fixed processing time for initialization. This results in increased power consumption, since this increases the time the device spends in processing (80-120mW) instead of deep sleep mode (0.48-0.67mW). The exact amount of increased power consumption can be measured, and this depends on the chirping parameters, frame rate, and sleep settings.

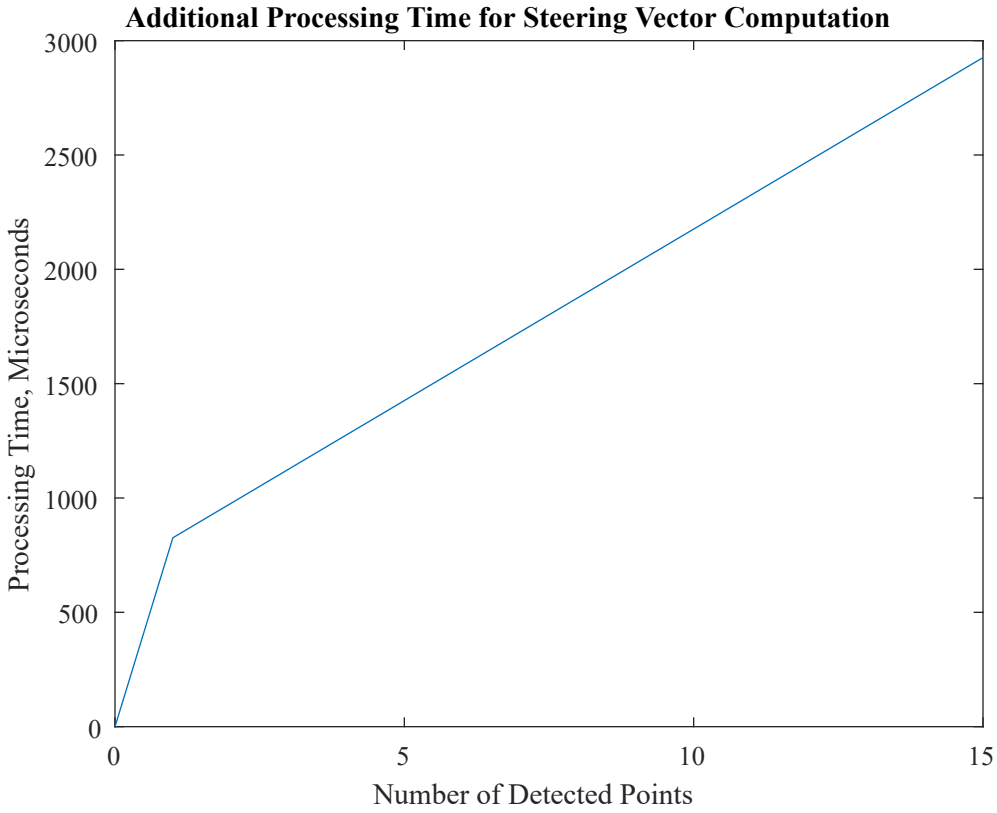

Figure 2-5. Processing Time vs # of Detected Points

2.4 Usage

TI developed a software tool that computes steering vector coefficients for the IWRL6432AOP for a given bandwidth and chirping frequency. The tool can be found in the MMWAVE-L-SDK under tools/steering_vector_generation_tool/. This can be run with the command:

```
generateSteeringVectors.exe --filename
"path\to\config.cfg" --azimSpacing %Azimuth_Spacing% --elevSpacing
%Elevation_Spacing%
```

See the readme in the same folder for more details about usage.

Once the steering vectors file (aoasv_table.c) is generated, this can be used in a CCS project one of two ways:

1. This can be copied (with all the files in the AOASVCDPU folder) into a CCS project, and built as a part of the CCS project. Note that the user can rename the .c file from *aoasv_table6432.c* to *aoasv_table.c*, and change some of the file paths in the AOASVCDPU and the CCS project to point to the new DPU. On MMWAVE-L-SDK 5.5.4, a folder called datapath/dpu/aoasvcproc/v0/ is needed to mimic the DPU folder structure found in motion_detect.h

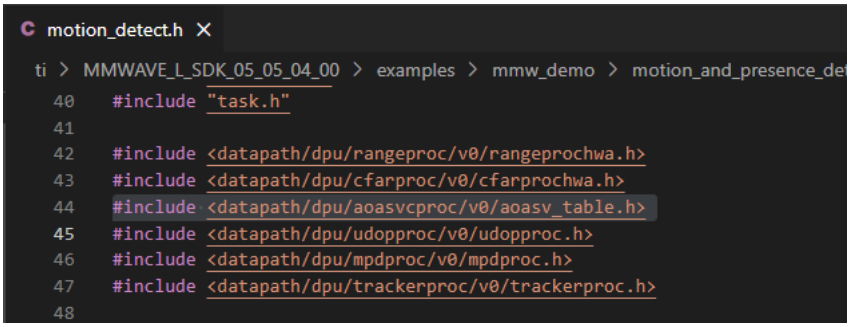

Figure 2-6. DPU Structure in motion_detect.h

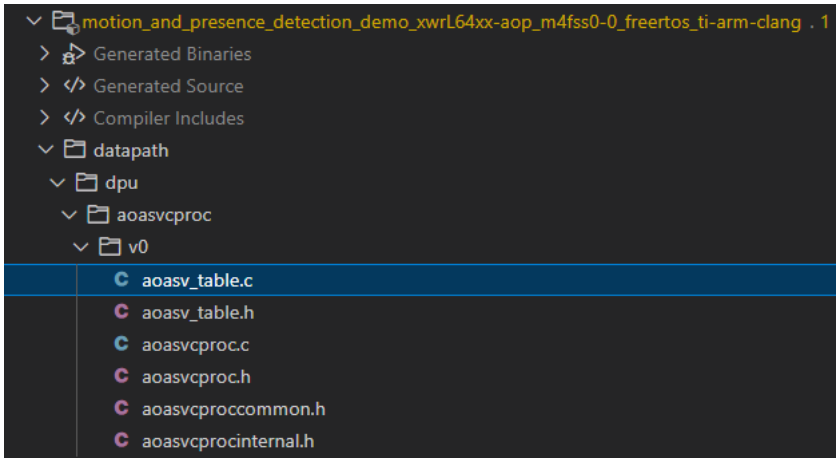

Figure 2-7. Folder Structure in Motion_and_Presence Project to Include AOASVCDPU

2. This can be built with a makefile as a part of the datapath DPU and linked to a CCS project.

2.5 Extensions to Other Platforms

The steering vectors package provided by TI is only relevant for the IWRL6432AOP device. This is because the coefficients are derived from gain and phase mismatch that is specific to the antenna design of the IWRL6432AOP. The coefficients are not compatible with other variants of the IWRL6432 (FCCSP and WCSP packages), AWRL6432, IWRL1432 or AWRL1432. TI does not support recollection of the steering vector coefficients for specific board designs and enclosures.

3 Summary

The IWRL6432AOP has two angle estimator methods. The FFT angle estimation algorithm offers good angle estimation performance within a reasonable field of view with quick processing times, whereas the Steering Vectors angle estimation algorithm offers improved angle estimation over a wider field of view, at the cost of slower processing times. The steering vectors algorithm was tested on stationary targets and walking human subjects over a wide bandwidth and frequency range to ensure robust performance across many conditions.

Both angle estimation algorothms allow designers to use the IWRL6432 to detect people and objects at long ranges. Looking forward, they could even be used together in a multi-pass detection architecture. The FFT angle estimation method can reduce the power consumption of the radar when people are not detected in the field of view, and upon detection, the steering vectors algorithm could offer finer localization to verify that the radar reacts properly depending on the location of the detections.

4 References

1. Texas Instruments, *The fundamentals of millimeter wave radar sensors*, marketing white paper.

5 Appendix

5.1 Chirping Parameters for Each Configuration File

Table 5-1. Full Chirping Parameters for Each Configuration

Configuration 1	channelCfg 7 3 0 chirpComnCfg 23 0 0 256 1 68 2 chirpTimingCfg 9.9 24 0 12.5 60.5 frameCfg 2 0 280 8 500 0
Configuration 2	channelCfg 7 3 0 chirpComnCfg 23 0 0 256 1 68 2 chirpTimingCfg 9.9 24 0 12.5 57.0 frameCfg 2 0 280 8 500 0
Configuration 3	channelCfg 7 3 0 chirpComnCfg 23 0 0 256 1 68 2 chirpTimingCfg 9.9 24 0 37.5 58.5 frameCfg 2 0 280 8 500 0
Configuration 4	channelCfg 7 3 0 chirpComnCfg 23 0 0 256 1 68 2 chirpTimingCfg 9.9 24 0 80 58 frameCfg 2 0 280 8 500 0

5.2 Point Cloud Data for Human Subject Testing

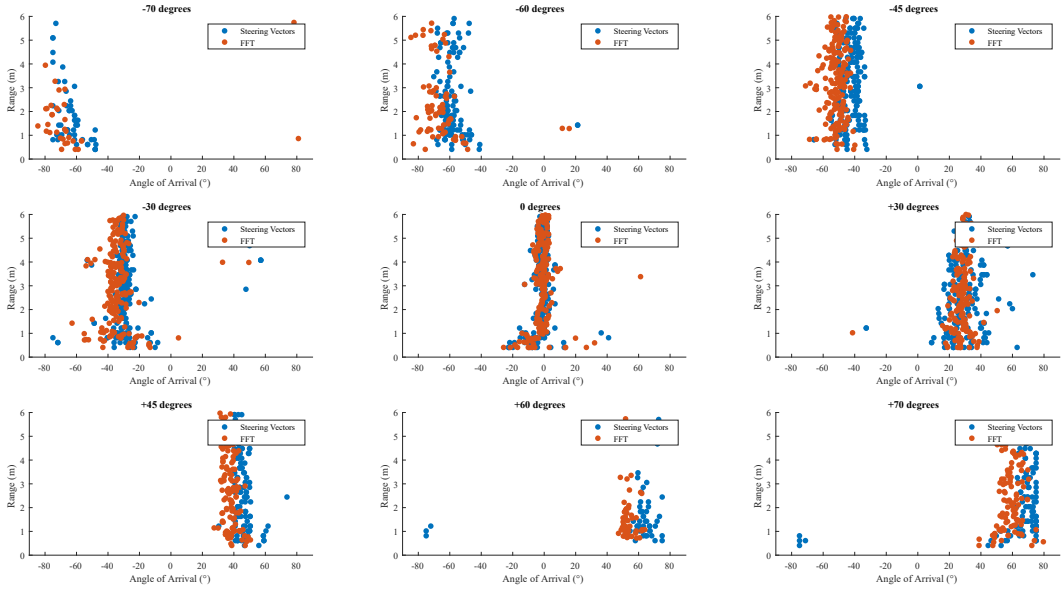

Figure 5-1. Walk Test, All Points Detected, Config 1

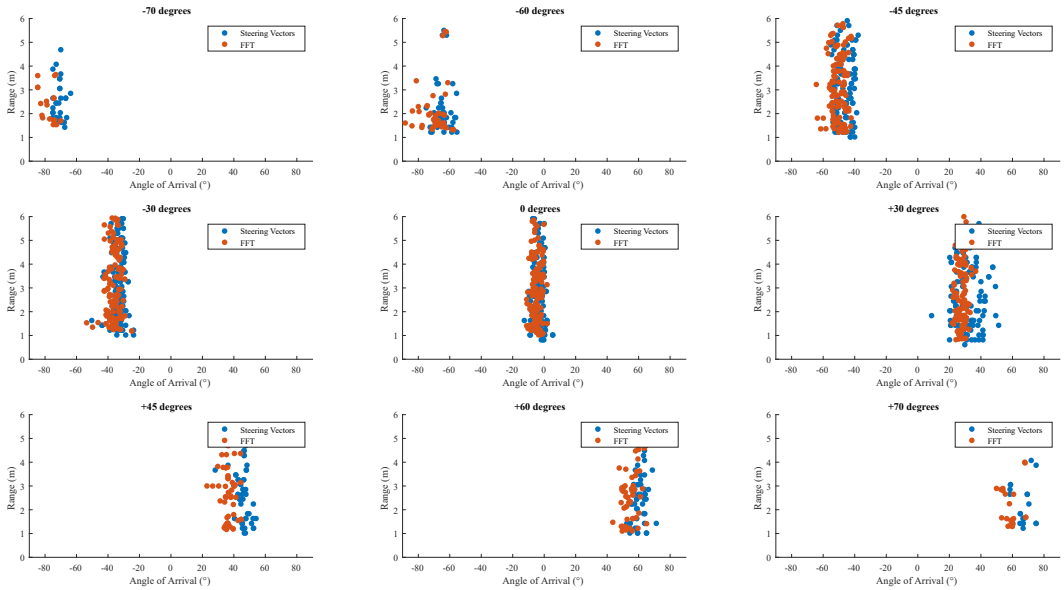

Figure 5-2. Walk Test, All Points Detected, Config 2

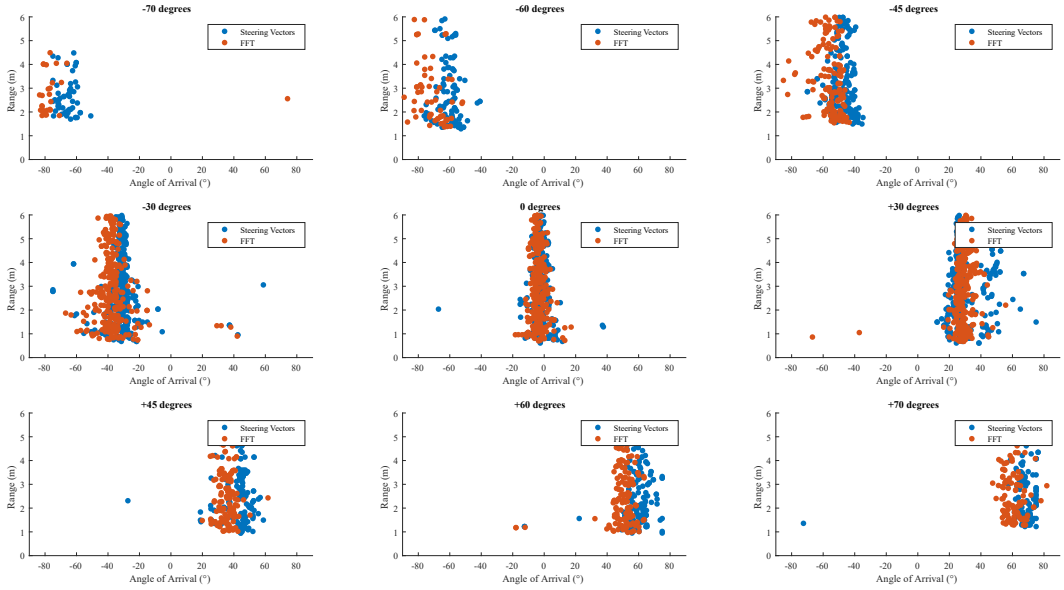

Figure 5-3. Walk Test, All Points Detected, Config 3

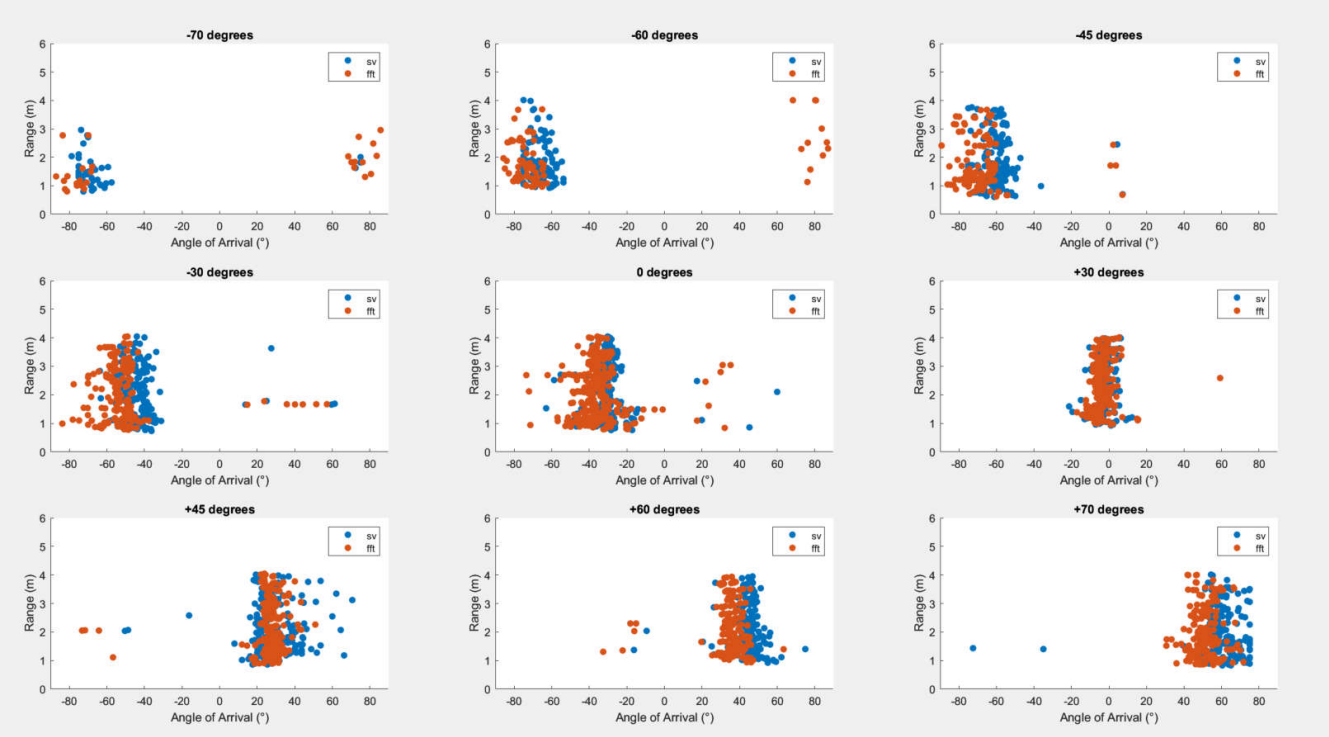

Figure 5-4. Walk Test, All Points Detected, Config 4

IMPORTANT NOTICE AND DISCLAIMER

TI PROVIDES TECHNICAL AND RELIABILITY DATA (INCLUDING DATA SHEETS), DESIGN RESOURCES (INCLUDING REFERENCE DESIGNS), APPLICATION OR OTHER DESIGN ADVICE, WEB TOOLS, SAFETY INFORMATION, AND OTHER RESOURCES “AS IS” AND WITH ALL FAULTS, AND DISCLAIMS ALL WARRANTIES, EXPRESS AND IMPLIED, INCLUDING WITHOUT LIMITATION ANY IMPLIED WARRANTIES OF MERCHANTABILITY, FITNESS FOR A PARTICULAR PURPOSE OR NON-INFRINGEMENT OF THIRD PARTY INTELLECTUAL PROPERTY RIGHTS.

These resources are intended for skilled developers designing with TI products. You are solely responsible for (1) selecting the appropriate TI products for your application, (2) designing, validating and testing your application, and (3) ensuring your application meets applicable standards, and any other safety, security, regulatory or other requirements.

These resources are subject to change without notice. TI grants you permission to use these resources only for development of an application that uses the TI products described in the resource. Other reproduction and display of these resources is prohibited. No license is granted to any other TI intellectual property right or to any third party intellectual property right. TI disclaims responsibility for, and you will fully indemnify TI and its representatives against, any claims, damages, costs, losses, and liabilities arising out of your use of these resources.

TI’s products are provided subject to TI’s Terms of Sale or other applicable terms available either on ti.com or provided in conjunction with such TI products. TI’s provision of these resources does not expand or otherwise alter TI’s applicable warranties or warranty disclaimers for TI products.

TI objects to and rejects any additional or different terms you may have proposed.

Mailing Address: Texas Instruments, Post Office Box 655303, Dallas, Texas 75265